Electrochemistry of Mitochondrial Isolates on Ultrasonicated Graphene Oxide-Modified Electrodes

Uriel Bruno-Mota[a], Safa Chaaben[a], Yuting Lei[a], Andrea Khouri[a,c], Claudia Champagne[b], Benjamin D. Ossonon[a], Emanuele Orgiu[a], Ian Gaël Rodrigue-Gervais[b]*, Ana C. Tavares[a]*

[a]Institut National de la Recherche Scientifique – Centre Energie Matériaux Télécommunications (INRS-EMT), 1650 Boulevard Lionel-Boulet, Varennes, Quebec, J3X 1P7, Canada.

[b]Institut National de la Recherche Scientifique – Centre Armand Frappier Santé Biotechnologie (INRS-AFSB), 531 Boulevard des Prairies, Laval, Quebec, H7V 1B7, Canada.

[c]McGill University – Biochemical Engineering Department, 845 Rue Sherbrooke Ouest, Montréal, Québec, H3A 0G4, Canada.

*Corresponding authors' contact information: ian.rodrigue-gervais@inrs.ca; ana.tavares@inrs.ca

Abstract

Mitochondria are central to cellular energy production and metabolic regulation, and their dysfunction is linked to various diseases. Understanding mitochondrial activity through electrochemical studies may provide valuable insights into their function, but direct characterization remains challenging due to the complexity of the electron transport chain (ETC) and the need to maintain mitochondrial integrity. While pyrolytic graphite (PGE) and carbon paper electrodes have been used in the past, the inherently weak and poorly resolved voltammetric signals from mitochondria complicate their electrochemistry.

This study investigates the use of PGE modified with graphene oxide obtained by electrochemical exfoliation of graphite (EGO) to enhance the electrochemical signals of isolated human mitochondria. To assess such activity, square wave voltammetry (SWV) was conducted in physiological conditions and compared with metabolic assays. The EGOs flakes and their suspensions obtained after different sonication times, and used in the fabrication of the electrodes were characterized by Scanning electron microscopy, X-ray photoelectron spectroscopy, transmission electron microscopy (TEM), and UV-vis spectroscopy.

TEM confirmed mitochondrial structural integrity after interaction with the EGO. Sonication time plays a critical control in mitochondrial viability and activity, as prolonged sonication yields smaller EGO flakes and more graphene oxide quantum dots (GOQD). The flakes improved the interaction between the mitochondria and the electrode's surface, whereas the GOQD facilitated the electron transfer between the ETC and the electrode, leading to stronger electrochemical signals. We highlight the importance of using SWV in combination with EGO and GOQD to resolve these signals more effectively, overcoming the limitations of typical voltammetry tests.

Keywords: Mitochondrial electrochemistry, Physiological-like conditions, Mitochondrial respiration, Graphene oxide, Graphene oxide quantum dots, Seahorse analysis, Square-wave voltammetry.

1. Introduction

The mitochondrion is perhaps the most studied organelle because its structure and function are central to cellular function, human health and disease [1,2]. Mitochondria have a complex structure consisting of a matrix delimited by an inner (IMM) and an outer (OMM) membrane [3]. One of the most important processes carried out by mitochondria is oxidative phosphorylation (OXPHOS), which generates adenosine triphosphate (ATP), the energetic currency of eukaryotic organisms. This process takes place at the inner mitochondrial membrane thanks to a group of multidomain protein complexes known as the electron transport chain (ETC) and the ATP synthase (**Scheme 1**). The ETC (Complexes I - IV) oxidizes hydrogen from carbohydrates, proteins and fats to fuel ATP production, generating water as a byproduct. As the electrons travel through complexes I, III and IV, a proton-induced electrochemical gradient is formed between the mitochondrial matrix and the intermembrane space. The proton movement generates a pH gradient and a membrane potential (ca. 150 mV) that serve as the driving force for the synthesis of ATP at the ATP-synthase [4]. As illustrated in **Scheme 1**, all protein complexes (I-IV) involved in the OXPHOS process carry out redox reactions of their substrates. Therefore, mitochondrial electrochemistry and fundamental knowledge on mitochondria-electrode communication are valuable tools to study the mitochondrial respiration. The development of electrochemically sensitive platforms offers significant potential for diagnosing mitochondrial-related diseases. These platforms would enable the study of biological entities without relying on fluorescent probes or the complex instrumentation required for standard techniques such as fluorescence resonance energy transfer, photo-induced electron transfer, intramolecular charge transfer, excited-state intramolecular proton transfer, surface-enhanced Raman scattering, and surface plasmon resonance [5].

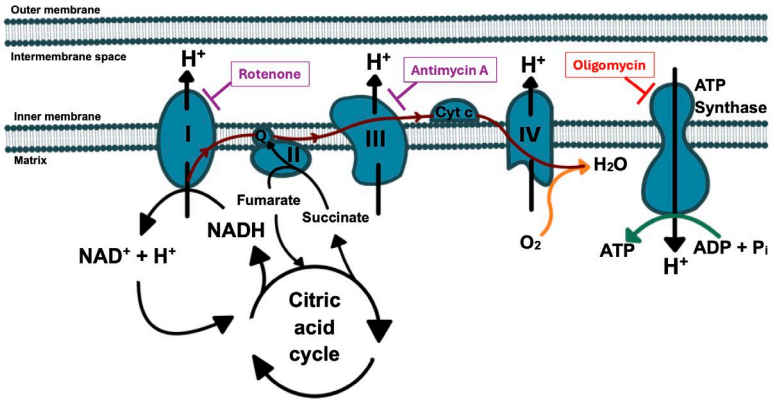

Scheme 1. *Representation of the oxidative phosphorylation process in mitochondria. The red arrow indicates the path of electrons in the electron transport chain, the orange arrow represents the reduction of oxygen at complex IV, and the green arrow shows the ATP synthesis at the end of the process. Inhibitors of the electron transport chain and their targets are indicated in purple and red.*

The electrochemistry of mitochondria has been subject of study over the last two decades after it was demonstrated that cyclic voltammograms with redox peaks can be recorded from the organelles drop casted on pyrolytic graphite electrodes [6]. For example, their ability to completely oxidize molecules was exploited in biofuel cells [7–9]. Also, several antibiotics, pesticides and explosive substances can target specifically the ETC inhibiting OXPHOS, which has been capitalized in the development of electrochemical biosensors for the detection of these harmful molecules [10–15].

Previous studies have explored the electrochemical response of mitochondria. Zhao *et. al* observed various voltametric peaks from isolated HeLa cell mitochondria on pyrolytic graphite electrodes (PGE). The authors attributed the signals to Cytochrome C (cyt c), to coenzyme Q (CoQ), or to FAD/$FADH_2$. These entities act as electron shuttles between the IMM and the electrode under an applied potential [6]. Later, Giroud *et. al* identified CoQ as the primary electron source responsible for redox signals in mitochondria from yeast, potato, and bovine heart [16]. They observed similar peaks with pure CoQ but none with pure cyt c. However, removing cyt c or CoQ from yeast, potato and bovine mitochondria decreased the redox peaks, suggesting that both contribute to the electrochemical signals. In fact, selective CoQ removal is challenging because of the affinity of ETC enzymes (eg. cyt c oxidase also known as complex IV) for organic solvents, as well as cyt c loss and mitochondrial structural disruption caused by KCl exposure during CoQ depletion protocol [17–19]. A more recent study revealed that mitochondrial handling, purification processes, and buffer composition significantly influence mitochondrial respiration and the electrochemical signals [20]. This effect is more pronounced in yeast, whose thick cell wall necessitates rigorous purification methods that often cause greater structural damage compared to mammalian mitochondria, which are typically isolated with minimal compromise [20]. Using yeast mutants (Δcyc3 and Δcox10 lacking cytochrome C and complex IV, respectively), the authors still found electrochemical signals present in the cyclic voltammograms, ruling out cyt c and complex IV as electron sources in yeast mitochondria. These findings align with those reported in [16].

Electrochemistry of mitochondria has been typically carried out using carbon-based working electrodes such as PGE [6] and carbon paper [12,15,16,20]. These materials have proven biocompatibility; however, weak signals are obtained with PGE, and the huge capacitive currents of carbon paper hinders the detailed study of the organelles, which, due to their structure, leads to low-intensity faradaic currents. Graphene-based materials have gained considerable attention during the last decades due to their intrinsic physicochemical properties and their broad applications in different fields, including biomedical sector [21,22]. Amongst them, graphene oxide (GO) stands out due to its unique properties which include high surface area, good mechanical strength, high conductivity, and remarkable hydrophilicity [22]. GO is rich in oxygenated functional groups distributed in different zones of the GO sheets. Moreover, the structure and toxicity of GO can be tuned using physical methods like ultrasonication or lyophilization [23], or chemical ones like the functionalization with organic molecules [24]. In the field of bioelectrochemistry, GO has found applications for the fabrication of enzymatic [25–27] and non-enzymatic [28,29] electrochemical biosensors, and for electrochemical immunosensors [30–32]. Additionally, GO functionalization has been used to facilitate biomarker detection which

has allowed the selective capture and release of cancerous cells [33,34]. However, to the best of our knowledge, the use of GO on the electrochemical response of subcellular structures has not yet been investigated.

In this work, electrochemical studies of mitochondria obtained from human cell lines are conducted in physiological conditions. They were chosen because they can be obtained in better health than those from yeast, and because electrochemical studies of human cells mitochondria are important for applications in diagnosis. Their response to different electrode materials (glassy carbon, pyrolytic graphite and GO obtained by electrochemical exfoliation of graphite) was investigated by both cyclic voltammetry and square wave voltammetry. Specific inhibitors of the ETC were used to identify the electrochemical signals associated with the mitochondria and the data corroborated with Seahorse analysis technique. It will be shown that the sonication time of the GO suspensions has a notable impact on the electrochemical response of the mitochondria. Ultimately, this work is a step forward to developing a reliable and simple electrochemical platform for monitoring human mitochondrial function.

2. Experimental

2.1. Synthesis and characterization of graphene oxide

Graphene oxide was synthesized by electrochemical exfoliation of a graphite foil, as outlined in [35]. Specifically, a graphite foil (7.5 cm × 2 cm × 0.05 cm) and a platinum mesh (6 cm^2) immersed in a 0.1 M H_2SO_4 electrolyte solution were connected to a direct current power supplier. The distance between the two electrodes was 6 cm and the potential difference between the electrodes was 10 V. The resulting graphene oxide flakes (named EGO) were collected via vacuum filtration using an MF-Millipore membrane with a pore size of 0.22 μm and subsequently washed multiple times with Millipore water to eliminate residual acid. The EGO flakes were redispersed in water through ultrasonication for 90 minutes, followed by freeze-drying to recover the powders. These EGO flakes were later used for the preparation of the suspensions described below.

Fresh suspensions of EGO at a concentration of 0.4 mg/mL were prepared by sonicating the EGO flakes in water for three hours. To evaluate the effect of the suspensions' sonication time on the mitochondrial respiration and electrochemical assays, these were subjected to additional sonication for a total of 3, 12, 20, 40, and 60 h. The samples were named as EGO-*x*h where *x* indicates the total sonication time in hours.

For characterization, the different suspensions of EGO were ultracentrifuged at 4500 g for 2 hours at room temperature to pellet the powders. The powders were allowed to dry at 37 ° C overnight before any characterization. Physicochemical characterization of the EGO-*x*h flakes was conducted by Scanning Electron Microscopy (SEM), X-Ray Photoelectron Spectroscopy (XPS). UV-vis spectrophotometry, Scanning Transmission Electron Microscopy (STEM), and High-Resolution Transmission Electron Microscopy (HR-TEM) were used for the characterization of the supernatants. See section 1.1 of the SI file for details.

2.2. Cell culture and mitochondrial purification

Two different working buffers were used for the experiments with mitochondria: Mitochondrial Purification Solution (MPS) that allows for purification of mitochondria with minimal damage and Mitochondrial Assay Solution (MAS) that contains all substrates that mitochondria need to sustain their activity for long periods of time [36]. See section 1.2 of the SI file for details about their composition.

Human embryonic kidney cells (HEK 293 ATCC number CRL-1573) were maintained in Dulbecco's Modified Eagle Medium (DMEM) medium supplemented with 10% heat inactivated fetal bovine serum, 1% penicillin-streptomycin, and 1% L-glutamine at 37 °C in 5% CO_2. The HEK293 cell line was chosen due to their fast growth.

Mitochondria from cultured cells were isolated as previously reported [37]: HEK293T cells were resuspended at 70 million mL^{-1} in cold MPS buffer solution designed to maintain a nearly isotonic environment. After a 30 min incubation on ice, the cells were forced through a 27-gauge needle 50–60 times. The homogenate was centrifuged 2 times (800 g, 20 min, 4°C) to remove nuclei, unbroken cells, and large membrane fragments. The mitochondrial fraction was pelleted by centrifugation of the post-nuclear supernatant at 8000 g for 20 min at 4 °C. The mitochondrial pellet was then washed with 200 µL of MPS and centrifuged once again at 8000 g for 20 min at 4 °C. The final mitochondrial pellet was resuspended in cold MAS buffer at a 400 mg/mL concentration (based on wet pellet weight). The mitochondrial proteins in the final mitochondrial suspension were quantified using the colorimetric DC protein assay (Bio-Rad®) using Bovine Serum Albumin (BSA) as protein standards. Typically, mitochondria were conserved in MAS at 4 °C overnight and plated for Seahorse analysis or drop-casted on the electrodes for electrochemistry the following day.

Transmission Electron Microscopy (TEM) imaging was used to ensure that mitochondrial structure was conserved after purification, and to evaluate the EGO-Mitochondria interactions. See section 1.3 of the SI file for more details on the sample preparation for microscopy.

2.3. Seahorse analysis

All Seahorse measurements were done using the Agilent Seahorse XFe96 extracellular flux analyzer. The oxygen consumption rate (OCR) of isolated mitochondria was measured in a 96-well plate format under basal conditions and after injection of drugs (see below). To minimize variability, mitochondria were diluted 10X in cold MAS and directly plated to a final loading of 10 µg (0.09 mg cm^{-2}) or 20 µg (0.18 mg cm^{-2}) of mitochondrial protein per well. The cell culture plate was then centrifuged at 2000 g for 20 minutes at 4 °C. Finally, the plate was transferred to a CO_2 free incubator and kept there for 1 h before starting the assay.

For the OCR measurements of mitochondria in presence of EGO, the wells of the cell culture plate were drop-casted with EGOs suspensions sonicated for different times and left to dry in a non-CO_2 incubator at 37 °C. Once dried, purified mitochondria were plated as described above. After centrifugation, the plates were kept at 4 °C overnight and transferred the next day to a non-CO_2 incubator at 37 ° for 1 h before measurements. For all Seahorse experiments, the ports A, B, C and

D of the Agilent Seahorse cartridge were loaded with 40 mM ADP, 40 µM Oligomycin (OM), 10 µM Carbonyl cyanide 4-(trifluoromethoxy) phenylhydrazone (FCCP) and 10 µM Rotenone / Antimycin A mix (RAA), respectively. The final well concentration for each drug was 4 mM ADP, 4 µM OM, 1 µM FCCP and 1 µM RAA.

2.4.Electrochemical analyses

For the electrochemical experiments, three different types of electrodes were considered: glassy carbon (GCE), edge plane oriented pyrolytic graphite (PGE) and drop-casted EGO-*x*h on PGE. Before measurements, the GCE and PGE were polished using 1 µm and 0.3 µm alumina powder. The electrodes were then rinsed with milli Q water and 70% ethanol. Finally, they were sonicated for 5 min in milli Q water, rinsed with 70% ethanol and let to dry.

For the experiments with EGO-*x*h, a loading of 85 µg/cm^2 of EGO-*x*h (at a concentration of 0.4 mg / mL) was drop-casted on the clean PGE and let dry at room temperature. For mitochondrial electrochemistry, a loading equivalent to 0.495 mg/ cm^{-2} of mitochondrial protein (ca. 2.5 to 5 × the loading for the Seahorse analysis to ensure detectable signals) was drop-casted on GCE, PGE, or PGE/EGO-*x*h and let dry for one hour. The mitochondria-functionalized electrodes were directly used as working electrodes during the electrochemical studies.

All electrochemical measurements were performed in a three-electrode electrochemical cell using an Ag/AgCl (1 M KCl) reference electrode and a Pt wire as a counter electrode. N_2 -saturated MAS solution, supplemented with 4 mM Adenosine diphosphate (ADP) to sustain the activity of the ETC was used as the electrolyte. All measurements were made using an Autolab PGSTAT 101. Cyclic voltammetry (CV) at 2 and 20 mVs^{-1} and square wave voltammetry (SWV) at a frequency of 40 Hz, step potential of 2 mV, and a modulation amplitude of 40 mV were used to characterize the electrochemical behavior of the isolated mitochondria. All SWV data were baseline-subtracted using MATLAB software (See section 1.4 of the SI file). The deconvolution of the SWV signals was done using Origin Lab software. To ensure consistency in the deconvolution of SWV signals, the full width at half maximum (FWHM) of the peaks associated with carbon materials was kept constant rather than fixing their positions. This approach preserves the integrity of peak assignments while allowing for natural potential shifts, providing a more reliable representation of the electrochemical processes at the electrode interface.

Scanning electron microscopy (SEM) imaging of mitochondria deposited on carbon screen printed electrodes was conducted to confirm their presence on the electrode surface after manipulation, as detailed in section 1.4 of the SI file.

3. Results and discussion

3.1.Measuring the electrochemical signals of mitochondrial isolates

Before the electrochemical measurements, transmission electron microscopy (TEM) imaging was employed to evaluate the mitochondrial integrity after the purification process. **Figure 1a** confirms that the mitochondria maintained their overall structural integrity, with no visible signs of damage. Well-defined cristae are observed, confirming that the internal architecture is preserved. A closer

examination in **Figure 1b** reveals the characteristic double membrane structure. Furthermore, **Figures 1c–f** illustrate that the presence of EGO, does not compromise the structural integrity of the mitochondria. The double membrane remains intact, and the cristae are still visible. This indicates that interactions with EGO, do not disrupt the mitochondrial morphology.

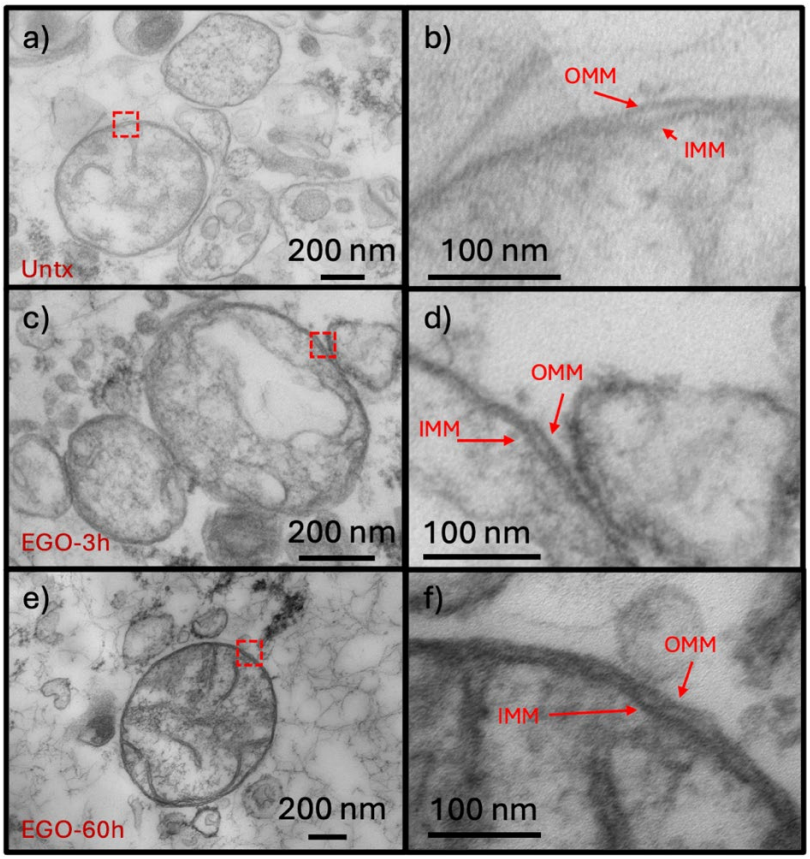

Figure 1*. TEM images of isolated mitochondria alone (Untx) (a), and in contact with EGOs sonicated for 3 h (c), and 60 h (e). (b), (d) and (f) are the corresponding close-up images at the dashed squares in a, b and c, where the details of the mitochondrial membranes can be observed.*

Cyclic voltammetry and square wave voltammetry were used to evaluate the electrochemical response of mitochondrial isolates immobilized on different electrode materials. Pyrolytic graphite electrodes (PGE) and glassy carbon electrodes (GCE) were used due to their stability, biocompatibility, and established use in bioelectrochemical studies. Electrochemically exfoliated graphene oxide (EGO) was selected for its large flake sizes and low density of defects, as reported by Lei *et al.* [35], which enhance the electrical conductivity and provide a surface optimized for electron transfer. The cyclic voltammograms in **Figures 2a** and **SI1** show the characteristic reversible peaks of the quinone functional groups of carbon materials between -0.16 and -0.10 V for the cathodic peak, and between 0.05 and 0.07 V for the anodic peak [38], but no peaks or signals that could be related to the mitochondria on GCE, PGE and PGE/EGO-60h (see the blank

cyclic voltammograms in **Figure SI2a**). These observations differ from the findings of Zhao *et. al* [6], who obtained weak reversible redox signals from isolated mitochondria from HeLa cells drop-casted on PGE. Although a direct comparison is not possible because the authors did not report the mitochondrial loading, the absence of such signals in our CVs might be due to the source of isolated mitochondria [16]. In this work, the mitochondria come from a different human cell line, and as previously reported different cell lines can exhibit variations in mitochondrial abundance and activity [39].

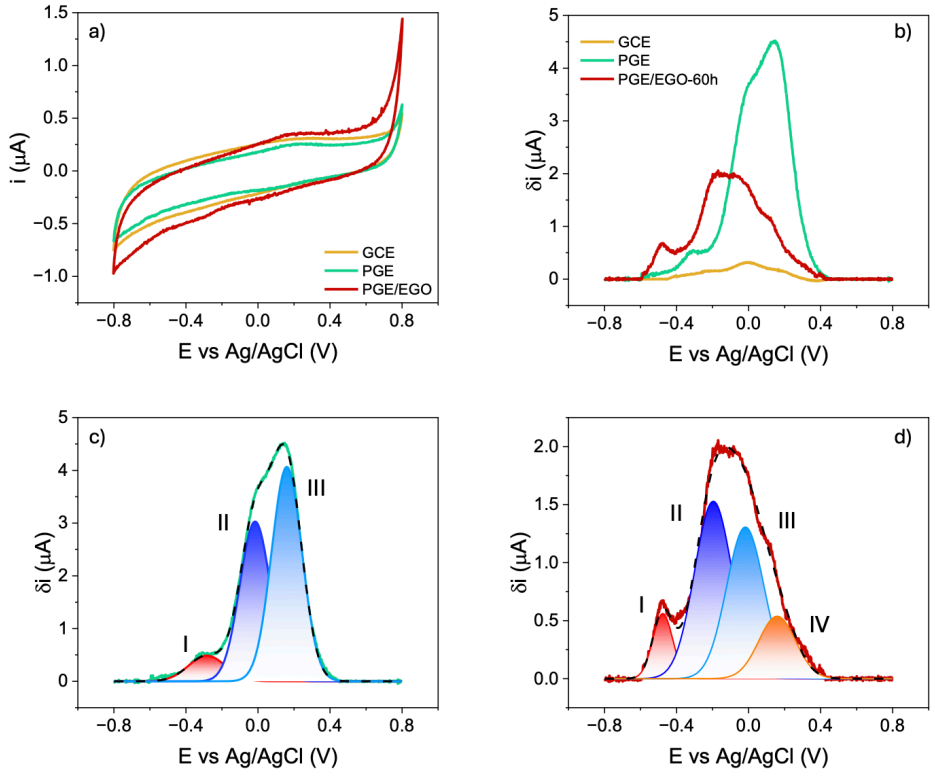

Figure 2. *a) Cyclic voltammograms in MAS buffer of drop-casted mitochondria on GCE, PGE and PGE/EGO-60h, and b) baseline subtracted square wave voltammograms in MAS buffer of drop-casted mitochondria on GCE, PGE and PGE/EGO-60h. See original non-subtracted data with and without mitochondria in* ***Figure SI3****. Peak deconvolution of the square wave voltammograms is shown in c) for PGE and in d) for PGE/EGO-60h. The dashed line corresponds to the cumulative fitting.*

However, as shown in **Figure 2b**, employing a more sensitive technique such as square wave voltammetry, reveals multiple peaks on the voltammograms of drop-casted mitochondria on the carbon electrodes. The peak potential and intensities depend on the nature of the electrode. A key factor contributing to the difference in signal intensity between electrodes with (**Figure 2b**) and without (**Figure SI2b**) mitochondria is the additional biological layer formed upon mitochondrial immobilization. SEM imaging of mitochondria-modified electrodes confirms the presence of

mitochondria on the electrode surface after experimental manipulation (**Figure SI4**). This demonstrates that mitochondria remain attached without the need for additional immobilization layers, ensuring that the observed electrochemical signals originate from the organelles themselves. This layer alters the electrochemical properties of the electrode, leading to a reduction in overall current. This effect is evident in **Figure SI5**, where the peak currents of the Ferri-Ferrocyanide redox probe decrease in the presence of mitochondria, confirming the formation of an additional interface. The SWV of mitochondria on GCE shows two small peaks at 0 and 0.2 V. Compared with the SWV of mitochondria on the GCE, the area under the curve for peak I at -0.28 V for mitochondria on PGE increased from 6.35×10^{-8} on the bare electrode (**Figure SI2d**) to 1.25×10^{-7} in presence of mitochondria (**Figure 2c**), while those of peaks II and III decreased from 1.87×10^{-6} and 3.98×10^{-6} to 6.37×10^{-7} and 8.58×10^{-7}, respectively. On the other hand, the whole signal of PGE/EGO-60h/Mitoc. is shifted by 200 mV to more negative potentials in comparison with the other two electrodes. The area under the curve of peak IV at 0.16 V increases from 7.84×10^{-9} for the PGE/EGO-60h electrode (**Figure SI2e**) to 1.38×10^{-7} when mitochondria are added (**Figure 2d**). This suggests that the presence of EGO enhances electron transfer from the mitochondria to the electrode, pointing for the advantage in using it as a support material for the direct electrochemistry of isolated mitochondria. To verify this hypothesis, cyclic voltammograms of the ferri-ferrocyanide redox probe ($[Fe(CN)_6]^{3-/4-}$) were recorded at different scan rates (See **Figure SI5**), and the the standard rate constant of electron transfer calculated using the Nicholson's method [40,41]. The following trend was found: 0.01137 ± 0.0012 cm s^{-1} (PGE/EGO) > 0.00346 ± 0.0001 cm s^{-1} (PGE/EGO/Mitoc.) > 0.00325 ± 0.0002 cm s^{-1} (PGE/Mitoc.). The k^0 on PGE/EGO/Mitoc. is slightly higher than on PGE/Mitoc. alone, supporting the idea that EGO contributes to facilitating electron transfer.

The SWVs of the bare GCE, PGE and PGE/EGO electrodes in MAS buffer solution are shown in **Figure SI2b**, and the deconvoluted signals in **Figure SI1 c-e**. Comparing the SWVs recorded with and without mitochondria, it is concluded that peaks II and III are related to the redox processes inherent to the carbon electrodes involving the oxygenated functional groups such as quinones [38], whereas peaks I and IV should be associated with the mitochondria. The peak potentials are reported in **Table S1**. The shift of peaks II and III to more negative potentials on PGE/EGO-60h in the presence of mitochondria observed in **Table S1** suggests higher local pH at the mitochondria-electrode interface. When mitochondria are active, they regulate local proton concentrations through their respiratory processes (see **Scheme 1)**. Due to the permeable nature of the OMM [42], protons can leak to the electrode surface. Since quinone groups on carbon materials (responsible for peaks II and III) undergo proton-coupled electron transfer, following the Nernst equation, their redox potential shifts in response to pH variations, explaining the observed negative shift when active mitochondria are on the electrode. On the other hand, peak I in **Figures 2c** and **2d** is at -0.28 V and -0.48 V for PGE/mitochondria and PGE/EGO-60h/mitochondria, respectively. Based on the literature this peak could be associated to the FAD/$FADH_2$ couple [6], to the CoQ [16,20], or to the cyt c [43], all of which are key elements of the ETC. Peak IV in **Figure 2d** is located at 0.16 V. In the works of Giroud *et. al* [16] and Koepke *et. al* [20], the oxidation of CoQ was assigned to the peaks found at 0.172 V - 0.222 V, 0.276 V and 0.134 V on the CVs of mitochondria isolated

from yeast, potato and bovine heart, respectively. It is worth mentioning that Zhang *et. al* also found a peak at -0.3 V when investigating the electrochemical response of active cytochrome C_3 immobilized on glassy carbon by square wave voltammetry and another one at -0.5 V corresponding to cytochrome C_3 in solution [43]. All peak potentials referenced from existing literature were converted to the Ag/AgCl reference electrode to facilitate comparison.

The complexity of the processes under investigation, combined with the varying sources of mitochondria and electrodes across different studies, make the identification of the source of electrochemical signals challenging. To verify that peaks I and IV are associated with the mitochondrial ETC and to determine their origins, specific inhibitors targeting the protein complexes involved in OXPHOS were employed. Before drop-casting, the mitochondrial isolates were exposed to 1 μM Rotenone-Antimycin A mixture (RAA) or 4 μM oligomycin (OM) overnight to specifically inhibit complexes I and III, or the ATP synthase (Complex V), respectively (See **Scheme 1**). **Figure 3a** shows the resulting SWVs.

Upon addition of RAA, mitochondrial activity is inhibited, reducing proton pumping to the intermembrane space and in consequence, a higher pH gradient at the OMM and EGO interface. This leads to a shift of peaks II, III, and IV to more positive values (See **Figure 3b**), peak I disappears, and the intensity of peak IV decreases by 96 %. As complexes I and III are inhibited, the flow of electrons towards the end of the ETC is hindered. Therefore, cyt c and complexes IV and V do not receive electrons and can no longer participate in mitochondrial respiration or in the electron transfer from the organelle to the electrode. Since succinate is present in the electrolyte, complex II should still be capable of transferring electrons to CoQ, which could, in principle, mediate electron transfer to the electrode. However, no signal is observed under these conditions, strongly suggesting that CoQ is not the primary contributor to the observed voltametric peaks. Furthermore, CoQ is embedded within the inner mitochondrial membrane (See **Scheme 1**) and is highly lipophilic [42], making its direct interaction with the electrode surface unlikely. In contrast, cytochrome c is a small, loosely bound, and water-soluble protein that can diffuse through the intermembrane space and interact with the electrode [44]. These findings do not completely discard CoQ as the responsible for the electron leak from the mitochondria to the electrode. But they suggest that in human cell lines, cyt c could be the main source of the electrochemical signals obtained from isolated mitochondria. This aligns with the studies of Zhang *et. al* [43] on the electrochemistry of cyt c on carbon materials, and of Zhao *et. al* [6] on the electrochemistry of mitochondria of another human cell line.

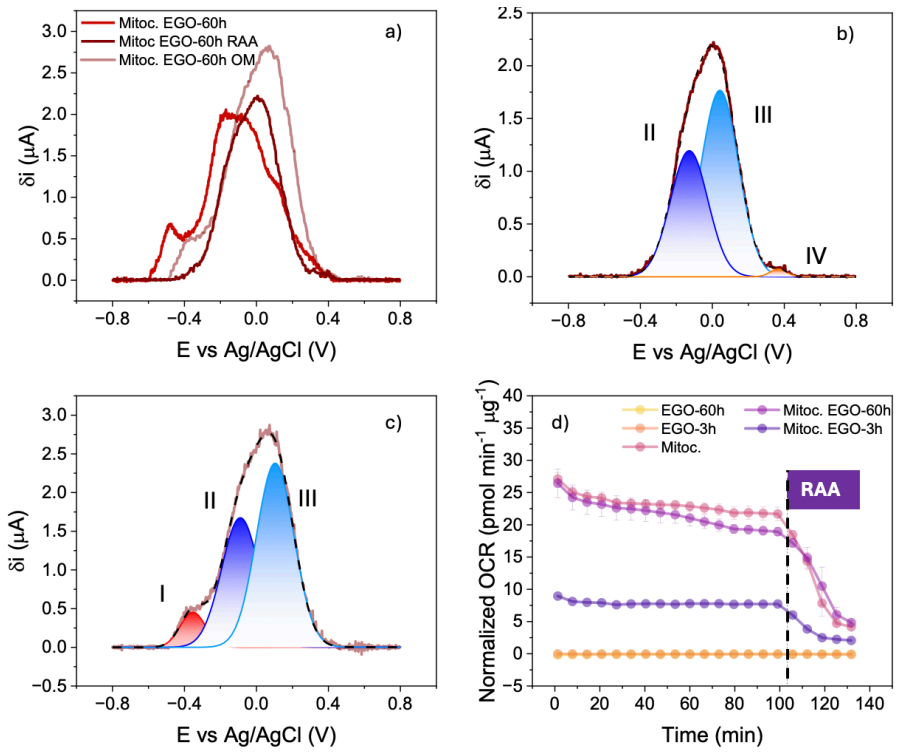

Figure 3*. a) Baseline-subtracted square wave voltammograms of drop-casted mitochondria on PGE/EGO-60h alone and in presence of oligomycin (OM) or rotenone-antimycin A mix (RAA). Unsubtracted data in* ***Figure SI7a****. The peak deconvoluted square wave voltammograms of mitochondria drop-casted on PGE/EGO-60h are shown in presence of RAA (b) and OM (c). MAS buffer was used as a working electrolyte. The Seahorse analysis of isolated mitochondria (20 μg of mitochondrial protein) alone and in presence of EGO-3h and EGO-60 h is shown in (d). The data average ± s. d. of 3 technical replicates is shown.*

With the addition of OM, peaks I-III shift positively by approximately 120 mV (**Figures 3a and 3c)**. This response is expected because a decrease in mitochondrial activity – in this case caused by inhibition of complex V - leads to a lower local pH at the OMM – electrode interface, due to the accumulation of protons at the intermembrane space that are not consumed by complex V,. Peak I does not disappear in this case because OM does not completely shut down the ETC but only inhibits the ATP-linked respiration. Some protons can still leak from the intermembrane space to the mitochondrial matrix and therefore complexes I to IV continue to work towards the formation of the electrochemical gradient. At the same time, peak III is now convoluted with peak IV as appreciated by the higher current intensity of peak III in **Figure 3a**.

The final electron acceptor of the electron transport chain is oxygen, and its reduction generates water (see **Scheme 1**, orange arrow). Thus, the activity of the ETC is routinely monitored by following the mitochondrial oxygen consumption. To validate the electrochemical data reported in **Figure 3a**, the oxygen consumption rate (OCR) of mitochondrial isolates was measured by Seahorse analysis. **Figure 3d** illustrates the basal respiration of isolated mitochondria alone and in

presence of EGO sonicated for 3 and 60 hours. As explained, the injection of RAA mixture specifically inhibits complexes I and III, hinders the transport of electrons and therefore the oxygen reduction. This shut down is observed in the decay of the OCR as appreciated in **Figure 3d**. This relates to the electrochemical data of **Figure 3b**. These findings validate that the electrochemical signals observed in **Figure 2** are originated at the ETC, most likely at cyt c. They also confirm that electrochemical methods can be used to assess the activity of the electron transport chain in human isolated mitochondria under physiological-like conditions.

Interestingly, the basal OCR of mitochondria in presence of EGO-3h is 65 % lower than the one recorded in the presence of EGO-60h. These two observations clearly indicate that the sonication time of the EGO has a direct influence on the activity of the ETC. The basal OCR of mitochondria alone and in contact with EGO-60h is the same at the beginning of the measurements, but start to diverge after about 40 min. More specifically, the OCR decreases in the presence of EGO over time and therefore long-term exposure of mitochondria to EGO is not recommended. During the electrochemical studies, mitochondria were in contact with the EGO for no longer than one hour before the measurements. The reduced basal mitochondrial respiration observed with EGO-3h, compared to EGO-60h and mitochondria alone, suggests that longer sonication times are less detrimental to mitochondrial respiration.

3.2. Effect of EGO's suspension sonication time on mitochondrial respiration

From section 3.1, it is evident that the electrochemical behavior of mitochondria is electrode dependent. Although the use of EGO seems to be advantageous to record electrochemical signals from isolated mitochondria, it is important to consider its effect on the mitochondrial respiration. **Figure 4a** shows the SWVs of isolated mitochondria drop-casted on PGEs modified with EGOs from suspensions sonicated for different times. The unsubtracted SWVs can be found in **Figure SI8**, and the deconvoluted ones in **Figure SI9.** The area under the four peaks is plotted in **Figure 4b**.

Peaks I and IV, associated with mitochondria, have clear trends with the suspensions' sonication time. The area under peak I increases with the sonication time, and its potential shifts from -0.39 V to -0.48 V. This negative shift in the potential values suggests a higher permeabilization of the OMM, facilitating the equilibration of proton concentration between the intermembrane space and the mitochondria-electrode interface, increasing the local pH. This permeabilization could allow for an easier migration of electroactive species and thus an enhanced electron transfer between mitochondria and the electrode surface when the EGO's suspension undergoes longer sonication. Similarly, the intensity of peak IV increases and the peak potential shifts from 0.29 V to 0.16 V. This pattern further supports the hypothesis that longer sonication times facilitate the electron transfer processes involving mitochondria on the electrode surface. The area under peaks II and III, associated with EGO, also initially increases with the sonication time up to 40 hours, indicating enhanced signal contributions from EGO. However, at 60 hours, a decline in these peak areas is observed, likely due to the overlapping of these EGO peaks with the increasingly prominent mitochondrial signals. Furthermore, the peak potentials for these EGO-related signals shift to more

negative values—from -0.09 V to -0.20 V for peak II and from 0.10 V to -0.02 V for peak III. The SWVs of drop-casted EGO on PGE electrodes without mitochondria are included in **Figure SI10**.

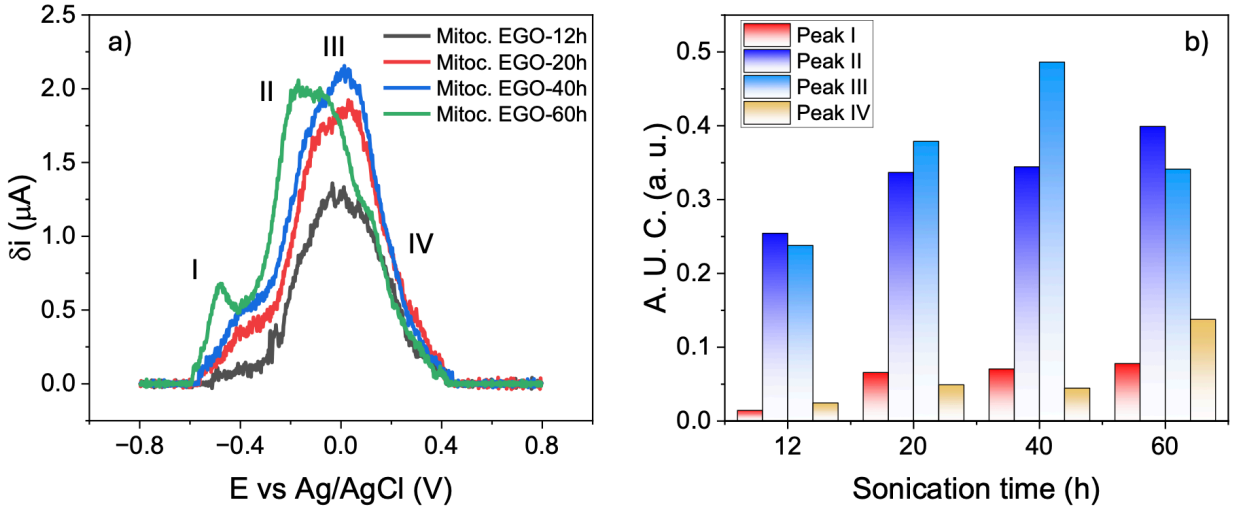

Figure 4. *a) Baseline subtracted SWV of drop-casted mitochondria on PGE modified with EGO sonicated for different times, in MAS buffer. Original data in* ***Figure SI8;*** *b) Area under the curve of the deconvoluted peaks in a). The longer the sonication time, the higher the area of the peaks associated to the mitochondria.*

Figure 5a shows the Seahorse results of isolated mitochondria alone and in presence of EGOs sonicated for different times. The various drugs were injected during the experiment to evaluate the response of the mitochondrial respiration. In all cases, and as expected, the addition of ADP substrate leads to higher OCR. After injection of OM, the OCR decreases because the ATP-synthesis-dependent OXPHOS has been shut down. When injecting the uncoupling agent trifluoromethoxyphenylhydrazone (FCCP), which modifies the proton permeability of the IMM, an increase in the OCR is observed. This is because protons are allowed to move freely across the inner membrane increasing the activity of complexes I-IV and the OCR. Finally, after injecting a mixture of rotenone and antimycin A (RAA), there is a complete shut-down of mitochondrial respiration and a drop in OCR is observed. The lack of distinction in basal respiration for the different conditions in **Figure 5a** may be attributed to the lower mitochondrial loading used in this experiment (10 μg) compared to the one in **Figure 3d** (20 μg), which reduces the sensitivity for detecting subtle differences. In **Figure 3d**, the higher mitochondrial concentration enhances the resolution of these variations, allowing for clearer distinctions in basal respiration. However, the large quantity of mitochondria required for such experiments poses significant experimental challenges, as obtaining sufficient mitochondrial isolates in consistent quality and quantity can be both time-consuming and technically demanding.

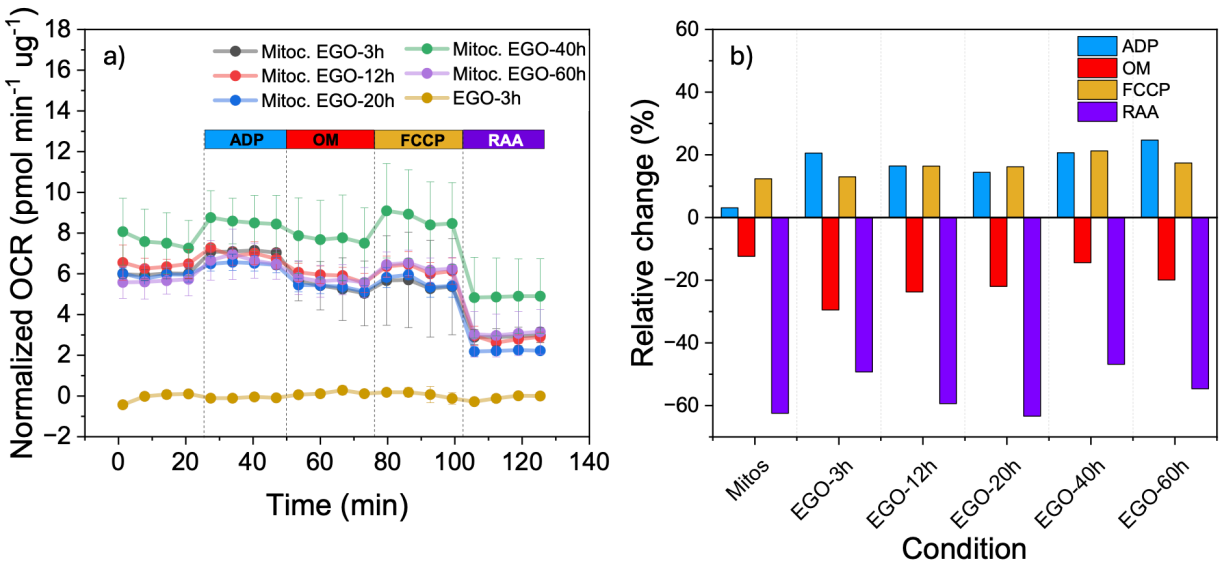

Figure 5 *a) Seahorse analysis of isolated mitochondria in presence of EGO sonicated for different times. The data average ± s. d. of 5 technical replicates is shown. b) Relative changes in the response of mitochondrial respiration to the injection of ADP as a substrate and different drugs that affect the ETC. Relative changes in mitochondrial respiration were calculated based on the lowest or highest OCR values observed in the preceding step.*

Even though the mitochondrial respiration profile looks qualitatively similar for all EGOs, **Figure 5b** shows that the OCR relative response to ADP and to each inhibitor varies with their sonication time. For ADP, a relative change of around 20% is observed in the presence of EGO indicating a higher permeability of the mitochondria to the substrate. The highest relative change was found for 60 h of sonication. This would suggest that the EGO interacts with the OMM allowing for a faster diffusion of ADP through the IMM and to the mitochondrial matrix where it serves as substrate for complex V to synthesize ATP. A consistent and similar effect is observed for OM, illustrated by the negative and high relative change in presence of EGO compared to mitochondria alone.

For FCCP, there is no significant difference between the relative response in presence and absence of EGO. This indicates that mitochondria are in a coupled state (IMM remains unaffected) even after exposure to the different EGOs. No considerable difference is neither observed for the response to RAA because these drugs simply shut down the ETC. The catalytic oxygen consumption by EGO itself can be discarded since the OCR response remains zero when mitochondria are not present as shown in **Figures 5a and SI11**. These findings are aligned with the electrochemical experiments where higher activity of the OCR was detected when mitochondria were in contact with EGO sonicated for longer times (**Figure 4a**).

3.3. EGO characterization and EGO-mitochondria interaction

Section 3.2 demonstrates that the suspensions' sonication time significantly impacts mitochondrial respiration and, consequently, their electrochemical signals. As shown in **Figure 1**, the TEM images do not reveal any obvious interaction between mitochondria and the graphene sheets reported in **Figure SI12a-c**. However, in the presence of EGO-3h and EGO-60h, the mitochondrial membranes exhibit a darker appearance compared to mitochondria alone. This contrast is particularly pronounced in the higher magnification images in **Figure 1b, d, and f**, where the inner mitochondrial membrane (IMM) and outer mitochondrial membrane (OMM) remain well-defined in the presence of EGO. By comparison, mitochondria that were not in contact with EGO show reduced contrast and a more blurred appearance. Moreover, mitochondria exposed to EGO-60h display a darker and blurrier intermembrane space compared to EGO-3h and mitochondria alone, suggesting greater material infiltration into the intermembrane space. This section explores the physicochemical properties of EGO subjected to varying sonication durations and examines how sonication influences the interaction between EGO and mitochondria.

Figure SI12a-c shows SEM images of the EGO flakes. It can be appreciated that longer sonication times reduces the flakes' size as already shown in the literature [45]. The XPS analysis (survey spectra shown in **Figure SI13**), revealed an increase of the C/O at% ratio with sonication time up to 40 h, followed by a decrease slight decrease for 60 h. As more or larger sp^2 carbon domains in the EGOs' basal plane are available, the interaction of the flakes with the biomolecules of the mitochondrial membrane through π-π bonding is facilitated, and the adhesion of the mitochondria to the electrode's surface improved [46,47]. Additionally, the smaller sheets generated with longer sonication time, provide a larger contact area between the EGO and the organelles' OMM.

Our results also suggest that other nanometric particles from the EGOs suspensions interact with the mitochondrial membranes. It has been reported that extended sonication of graphene materials in suspension leads to the formation of graphene oxide quantum dots (GOQD) that absorb in the ultraviolet [48,49]. To investigate the formation of GOQD, the EGO suspensions used for mitochondrial electrochemistry were centrifuged to precipitate and remove the large EGO sheets. UV-vis spectra of the supernatants were recorded, and STEM and HR-TEM images of the particles therein obtained. The spectra reported in **Figure 6a** show two peaks at 202 and 263 nm suggesting the presence of GOQD [48]. Moreover, their intensity increases with the sonication time, indicating a larger concentration. **Figures 6b-c** show the TEM images of the particles present in the EGO-40h and EGO-60h supernatants. The presence of both EGO flakes (dimensions above 20 nm) and GOQDs (20 nm or smaller) are observed in both figures, but larger and more abundant flakes were found in the EGO-40h suspension compared to EGO-60h. These observations are consistent with the UV-vis results, where the increasing peak intensities with longer sonication times indicates a higher concentration of GOQDs. **Figure 6d** displays a high resolution (HR-TEM) image of a GOQD from the EGO-60h supernatant, with the inset confirming a lattice parameter of 0.204 nm -consistent with previously reported values for GOQDs [50]. This aligns with the TEM images in **Figure 1** where darker membranes and greater infiltration of nanosized structures into the intermembrane space is observed with the sonication time.

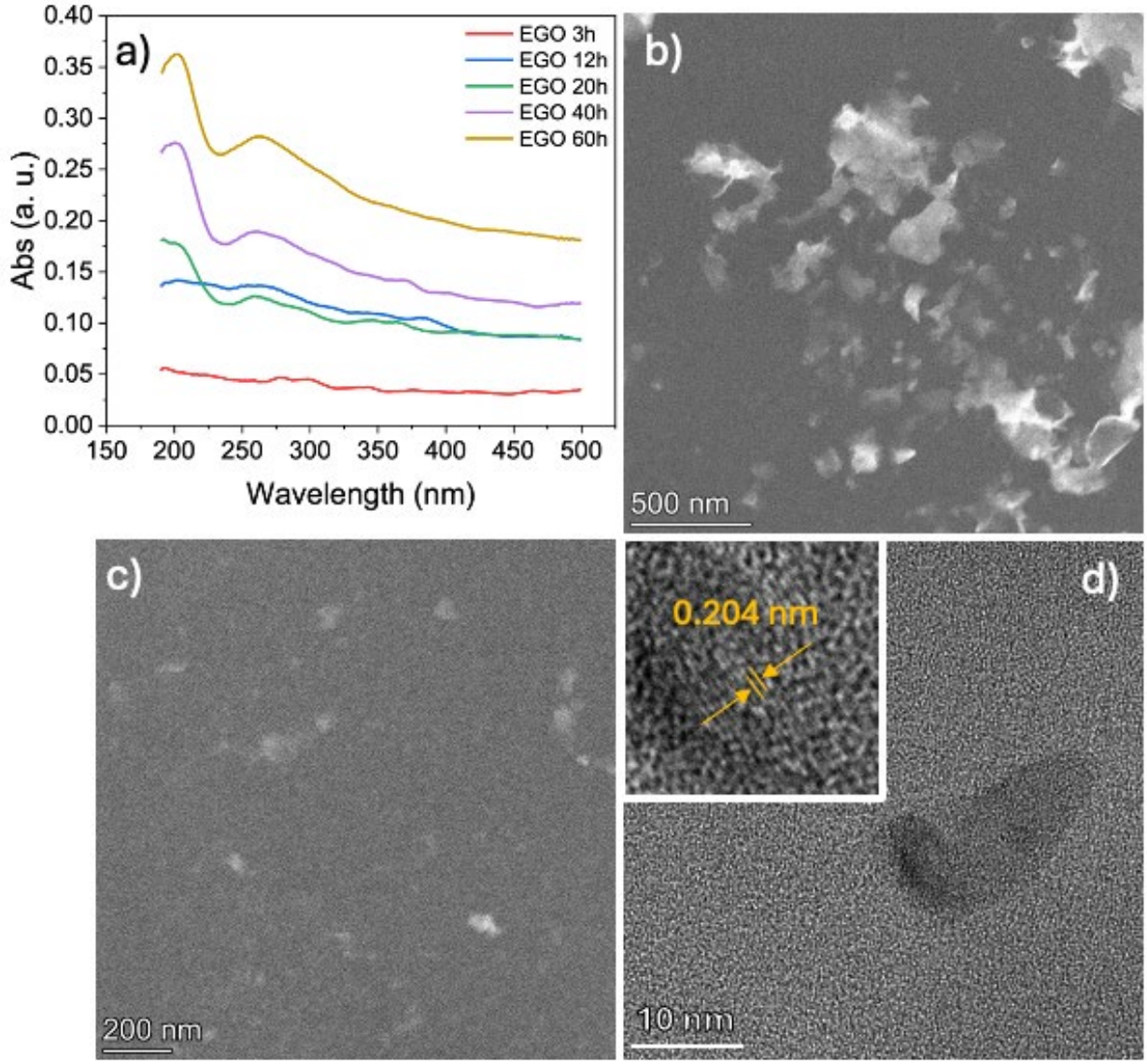

***Figure 6**. a) UV-vis spectra of the GOQD generated by EGO sonication for different times. Longer sonication times yield higher concentrations of GOQDs; STEM images of the EGO flakes and GOQD present in the b) EGO-40h and c) EGO-60h supernatants; d) HR-TEM image of a GOQD present in the EGO-60h supernatant. The inset shows a higher magnification image with the lattice d-spacing.*

To evaluate the role of these GOQD on the electrochemical signals of mitochondria, additional SWVs were recorded with PGE modified with the supernatant solution from EGO-60h and with and without mitochondria. As shown in **Figure SI14a,** the mitochondria in the presence of GOQD (supernatant) exhibit a similar electrochemical response to that observed with EGO-60h with four peaks in the SW voltammogram. Moreover, the peaks position is shifted to more negative

potentials compared to PGE/Mitoc. (**Figure SI14a and Figure 2b**). Notably, the SWV of PGE/GOQD (no mitochondria) shows peaks II, III and IV, suggesting that GOQD may be partially responsible for peak IV (**Figure SI14b**). Although peak IV is present, its area increases from 7.2 $\times 10^{-8}$ to 1.07×10^{-7} when mitochondria are present (**Figure SI14c**), further supporting the hypothesis that mitochondria contribute to peak IV.

Liao *et. al* [45], showed that the size of graphene oxide particles correlates with their interaction with the cell membrane. Smaller particles present stronger electrostatic interactions with the lipid bilayer. The electrostatic interaction between GOQD with mitochondria most likely alters the permeability of the OMM, facilitating the diffusion of ADP into the mitochondrial matrix, as suggested by the results in **Figure 5b**. However, the permeability of the IMM most likely is not altered since the mitochondrial respiration is not affected, as shown in the Seahorse analysis experiments, particularly with the response to FCCP, **Figure 5b**. The OMM is known to be more permeable than the IMM due to its high content of porins, which form β-barrel channels that allow the passive diffusion of molecules up to ~5 kDa. In contrast, the IMM is highly selective and impermeable to most ions and small molecules, as it is rich in cardiolipin and tightly packed protein complexes responsible for oxidative phosphorylation [42]. The GOQD might serve a role similar to digitonin that is used to permeabilize the OMM, enabling substrates such as pyruvate to access the mitochondria while preserving the integrity of the IMM and maintaining OCR [51]. In terms of electrochemical communication between the organelle and the electrodes, the membrane's permeabilization by the GOQD would allow for an easier diffusion of the cyt c from the IMM to the electrode's surface and possibly act as a shuttle for cyt c.

Conclusions

This study demonstrates the potential of use of EGO as a versatile platform for the immobilization and electrochemical characterization of mitochondrial isolates in physiological conditions and without additional immobilization layers. Mitochondrial signals were reliably detected on PGE, PGE modified with EGO, and PGE modified with GOQD, while GCE failed to yield measurable signals. The structural properties of EGO, such as the sheet size, were found to be useful in modulating mitochondrial adhesion to the electrode. Longer sonication times of EGO' suspensions produced GOQD that interact with the mitochondrial membranes and facilitate the electron transfer between the mitochondrial ETC and the electrode's surface.

Metabolic assays confirmed that mitochondria exposed to EGO sonicated for longer time exhibited higher basal respiration, resulting in enhanced biocompatibility for the electrochemical studies. Inhibitor studies identified cytochrome C as the most likely primary electron mediator between the ETC and the electrode, reinforcing EGO and GOQD as a potential tool for probing mitochondrial function. While the findings underscore the promise of these materials for bioelectrochemical applications, challenges remain in improving signal resolution and sensitivity to enable quantitative analyses. Future research should explore optimizing electrode configurations, such as ultramicroelectrodes, and further tailoring the materials composition and structural properties to

advance the understanding of mitochondrial dysfunction and its role in disease.

CRediT author statement

Uriel Bruno-Mota: Conceptualization, Methodology, Data curation, Formal analysis, Investigation, Visualization, Writing – original draft. **Safa Chaaben:** Investigation, Visualization, Writing - Review & Editing. **Yuting Lei:** Investigation, Writing - Review & Editing. **Andrea Khouri:** Data curation, Formal analysis, Software. **Claudia Champagne:** Methodology, Writing - Review & Editing. **Benjamin Ossonon:** Methodology, **Emanuele Orgiu:** Supervision, Writing - Review & Editing. **Ian Gaël Rodrigue-Gervais:** Conceptualization, Supervision, Writing - Review & Editing. **Ana C. Tavares:** Conceptualization, Funding acquisition, Project administration, Supervision, Writing - Review & Editing.

Declaration of competing interests

None of the authors have competing conflicts of interests to declare.

Acknowledgements

ACT and EO acknowledge the financial support from Natural Sciences and Engineering Research Council of Canada (NSERC) Discovery grant program. IGRG acknowledges the financial support from NSERC (RGPIN-2017-06568) and Fonds de Recherche du Québec (FRQ, Établissement de jeunes chercheurs 265327). UBM acknowledges the scholarships from FRQ (Doctoral research scholarship 312640) and Consejo Nacional de Humanidades Ciencias y Tecnologia (Scholarship CONAHCYT 771722 for studies abroad). SC acknowledges the scholarship from the Tunisian University Mission in North America (MUTAN, Tunisia). AK acknowledges the URSA scholarship from NSERC. The authors acknowledge Prof. Laurent Chatel-Chaix (INRS-AFSB) for providing access to the Seahorse XFe96 Extracellular Flux Analyzer and for providing some of the materials for Seahorse Analysis and cell culture, Prof. Daniel Guay (INRS-EMT) for granting access to the UV-vis spectrophotometer, Laura Daniela Tejeda-Valencia (INRS-AFSB) and Prof. Stéphane Lefrançois (INRS-AFSB) for providing HEK293 cells for the experiments. Transmission electron microscopy imaging of isolated mitochondria and scanning electron microscopy of mitochondria-modified electrodes were performed in the INRS-AFSB Electron Microscopy Facility (“Plateforme de caractérisation des nanovéhicules biologiques ou de synthèse”). The authors thank Dr. Angel Valdez at the Facility for Electron Microscopy Research of McGill University for help in transmission electron microscope operation and data collection.

Data availability

Data will be made available on request.

Declaration of generative AI and AI-assisted technologies in the writing process

During the preparation of this work the author(s) used Copilot in order to improve the clarity of certain paragraphs. After using this tool/service, the author(s) reviewed and edited the content as needed and take(s) full responsibility for the content of the publication.

References

[1] N.L. Frantz, G. Brakoniecki, D. Chen, D.A. Proshlyakov, Anal Chem 93 (2021) 1360–1368.

[2] A.K. Kondadi, A.S. Reichert, Annu Rev Biophys 53 (2024) 147–168.

[3] T.G. Frey, C.A. Mannella, Trends Biochem Sci 0004 (2000) 319–324.

[4] C.H. Lee, D.C. Wallace, P.J. Burke, ACS Nano 18 (2024) 1345–1356.

[5] W. Ji, X. Tang, W. Du, Y. Lu, N. Wang, Q. Wu, W. Wei, J. Liu, H. Yu, B. Ma, L. Li, W. Huang, Chem Soc Rev 51 (2022) 71–127.

[6] J. Zhao, F. Meng, X. Zhu, K. Han, S. Liu, G. Li, Electroanalysis 20 (2008) 1593–1598.

[7] R.L. Arechederra, K. Boehm, S.D. Minteer, Electrochim Acta 54 (2009) 7268–7273.

[8] D. Bhatnagar, S. Xu, C. Fischer, R.L. Arechederra, S.D. Minteer, Physical Chemistry Chemical Physics 13 (2011) 86–92.

[9] R. Arechederra, S.D. Minteer, Electrochim Acta 53 (2008) 6698–6703.

[10] M.N. Germain, R.L. Arechederra, S.D. Minteer, J Am Chem Soc 130 (2008) 15272–15273.

[11] M.N. Arechederra, C.N. Fischer, D.J. Wetzel, S.D. Minteer, Electrochim Acta 56 (2010) 938–944.

[12] T. Wang, R.C. Reid, S.D. Minteer, Electroanalysis 28 (2016) 854–859.

[13] S.L. Maltzman, S.D. Minteer, Analytical Methods 4 (2012) 1202–1206.

[14] R.L. Arechederra, A. Waheed, W.S. Sly, C.T. Supuran, S.D. Minteer, Bioorg Med Chem 21 (2013) 1544–1548.

[15] T. Wang, S.D. Minteer, J Electrochem Soc 163 (2016) H1047–H1052.

[16] F. Giroud, T.A. Nicolo, S.J. Koepke, S.D. Minteer, Electrochim Acta 110 (2013) 112–119.

[17] G. Ayala, A. Nascimento, A. Gómez-Puyou, A. Darszon, Biochimica et Biophysica Acta (BBA) - Bioenergetics 810 (1985) 115–122.

[18] S. Mishra, R. Mishra, Int J Proteomics 2015 (2015) 1–12.

[19] L. Szarkowska, Arch Biochem Biophys 113 (1966) 519–525.

[20] S.J. Koepke, J.J. Watkins, S.D. Minteer, J Electrochem Soc 163 (2016) H292–H298.

[21] R.G. Bai, R. Tuvikene, Handbook of Carbon-Based Nanomaterials (2021) 551–571.

[22] S. Yadav, A.P. Singh Raman, H. Meena, A.G. Goswami, Bhawna, V. Kumar, P. Jain, G. Kumar, M. Sagar, D.K. Rana, I. Bahadur, P. Singh, ACS Omega 7 (2022) 35387–35445.

[23] J. Schmuck, W. Rondan, U. Reno, J. Vasquez, L. Regaldo, A.M. Gagneten, A. Champi, Diam Relat Mater 145 (2024) 111145.

[24] Y. Lei, L. dos S. Madalena, B.D. Ossonon, F.E.B. Junior, J. Chen, M.R.V. Lanza, A.C. Tavares, Molecules 27 (2022) 7629.

[25] T. Madasamy, C. Santschi, O.J.F. Martin, Analyst 140 (2015) 6071–6078.

[26] T. Madasamy, M. Pandiaraj, M. Balamurugan, K. Bhargava, N.K. Sethy, C. Karunakaran, Biosens Bioelectron 52 (2014) 209–215.

[27] M. Pandiaraj, T. Madasamy, P.N. Gollavilli, M. Balamurugan, S. Kotamraju, V.K. Rao, K. Bhargava, C. Karunakaran, Bioelectrochemistry 91 (2013) 1–7.

[28] M. Thangamuthu, W.E. Gabriel, C. Santschi, O.J.F. Martin, Sensors 2018, Vol. 18, Page 800 18 (2018) 800.

[29] K.J. Huang, Q.S. Jing, Z.W. Wu, L. Wang, C.Y. Wei, Colloids Surf B Biointerfaces 88 (2011) 310–314.

[30] A.A. Saeed, J.L.A. Sánchez, C.K. O'Sullivan, M.N. Abbas, Bioelectrochemistry 118 (2017) 91–99.

[31] J. Wang, X. Wang, H. Tang, Z. Gao, S. He, J. Li, S. Han, Biosens Bioelectron 100 (2018) 1–7.

[32] Q. Zhu, Y. Chai, Y. Zhuo, R. Yuan, Biosens Bioelectron 68 (2015) 42–48.

[33] H.J. Yoon, T.H. Kim, Z. Zhang, E. Azizi, T.M. Pham, C. Paoletti, J. Lin, N. Ramnath, M.S. Wicha, D.F. Hayes, D.M. Simeone, S. Nagrath, Nature Nanotechnology 2013 8:10 8 (2013) 735–741.

[34] H.J. Yoon, A. Shanker, Y. Wang, M. Kozminsky, Q. Jin, N. Palanisamy, M.L. Burness, E. Azizi, D.M. Simeone, M.S. Wicha, J. Kim, S. Nagrath, Adv Mater 28 (2016) 4891.

[35] Y. Lei, B.D. Ossonon, J. Chen, J. Perreault, A.C. Tavares, Journal of Electroanalytical Chemistry 887 (2021) 115084.

[36] R.J. Romani, S. Ozelkok, Plant Physiol 51 (1973) 702–707.

[37] M.C. Landry, C. Champagne, M.C. Boulanger, A. Jetté, M. Fuchs, C. Dziengelewski, J.N. Lavoie, Journal of Biological Chemistry 289 (2014) 2230–2249.

[38] M. Lu, R.G. Compton, Analyst 139 (2014) 4599–4605.

[39] S. Michel, A. Wanet, A. De Pauw, G. Rommelaere, T. Arnould, P. Renard, J Cell Physiol 227 (2012) 2297–2310.

[40] R.S. Nicholson, Anal Chem 37 (1965) 1351–1355.

[41] I. Lavagnini, R. Antiochia, F. Magno, Electroanalysis 16 (2004) 505–506.

[42] M. Giacomello, A. Pyakurel, C. Glytsou, L. Scorrano, Nature Reviews Molecular Cell Biology 2020 21:4 21 (2020) 204–224.

[43] D. Zhang, G.S. Wilson, K. Niki, Anal Chem 66 (1994) 3873–3881.

[44] P. Bernardi, G.F. Azzone, Journal of Biological Chemistry 256 (1981) 7187–7192.

[45] K.H. Liao, Y.S. Lin, C.W. MacOsko, C.L. Haynes, ACS Appl Mater Interfaces 3 (2011) 2607–2615.

[46] B. Zhang, P. Wei, Z. Zhou, T. Wei, Adv Drug Deliv Rev 105 (2016) 145–162.

[47] V. Georgakilas, M. Otyepka, A.B. Bourlinos, V. Chandra, N. Kim, K.C. Kemp, P. Hobza, R. Zboril, K.S. Kim, Chem Rev 112 (2012) 6156–6214.

[48] L. Lu, Y. Zhu, C. Shi, Y.T. Pei, Carbon N Y 109 (2016) 373–383.

[49] S. Zhuo, M. Shao, S.T. Lee, ACS Nano 6 (2012) 1059–1064.

[50] B. Karimi, B. Ramezanzadeh, J Colloid Interface Sci 493 (2017) 62–76.

[51] A.E. Vercesi, C.F. Bernardes, M.E. Hoffmann, F.R. Gadelha, R. Docampo, Journal of Biological Chemistry 266 (1991) 14431–14434.